Vol 18 No 12, December 2009
1674-1056/2009/18(12)/5451-06

Chinese Physics B

© 2009 Chin. Phys. Soc.
and IOP Publishing Ltd

A theoretical study of harmonic generation in a short period AlGaN/GaN superlattice induced by a terahertz field

Chen Jun-Feng(陈军峰)† and Hao Yue(郝 跃)

Key Laboratory of the Ministry of Education for Wide Band-Gap Semiconductor Materials and Devices, School of Microelectronics, Xidian University, Xi'an 710071, *China*

(Received 22 June 2009; revised manuscript received 21 August 2009)

Based on an improved energy dispersion relation, the terahertz field induced nonlinear transport of miniband electrons in a short period AlGaN/GaN superlattice is theoretically studied in this paper with a semiclassical theory. To a short period superlattice, it is not precise enough to calculate the energy dispersion relation by just using the nearest wells in tight binding method: the next to nearest wells should be considered. The results show that the electron drift velocity is 30% lower under a dc field but 10% higher under an ac field than the traditional simple cosine model obtained from the tight binding method. The influence of the terahertz field strength and frequency on the harmonic amplitude, phase and power efficiency is calculated. The relative power efficiency of the third harmonic reaches the peak value when the dc field strength equals about three times the critical field strength and the ac field strength equals about four times the critical field strength. These results show that the AlGaN/GaN superlattice is a promising candidate to convert radiation of frequency ω to radiation of frequency 3ω or even higher.

Keywords: terahertz, GaN, superlattice, nonlinear transport
PACC: 7230, 7360L, 7210

1. Introduction

The terahertz (THz) regime, which corresponds to the frequency range from 100 GHz to 10 THz (3 mm to 30 μm wavelength), has attracted much attention in recent decades because it offers many special advantages over the traditional frequency regime. Recently, theories and experiments have been developed for the promising application of THz in biological and medical imaging, broadband and safety communication, radar, space science, etc.[1−4] There are two ways to obtain THz radiation. From the low side of the THz frequency electronic based devices such as Gunn diodes, impact avalanche transit time diodes, and resonant tunnelling diodes are widely investigated.[5−8] From the high side, photonics based devices such as quantum cascade lasers extend the emission wavelength from mid- and far-infrared to the THz spectrum range.[9−12]

Currently, THz devices are mainly fabricated with GaAs material. The output power and the operation temperature of these devices are limited by the intrinsic property of the GaAs material. The GaN material is famous for its high critical field (2 MV/cm), electron saturation velocity (2×10^7 cm/s) and higher thermal conductivity (1.3 W/cm·K). These advantages allow for the high output power and operation temperature, thus the GaN material may be one of the best candidates for fabricating THz devices. In this paper, the high harmonic response of a short period AlGaN/GaN superlattice under a THz field is investigated with emphasis on the relations of the third harmonic amplitude, phase, power efficiency and the frequency, strength of the THz electric field.

2. Model

2.1. Energy dispersion relation of the short period AlGaN/GaN superlattice

Consider a planar superlattice, in which electrons travel along the growth direction (z axis) through the lowest miniband formed by the periodically spaced potential wells and barriers. Electrons move freely in the lateral plane (x and y directions), the energy is the same as that of the free electrons $\varepsilon_{k\|} = k_\|^2/2m$, while the energy along the z direction is quantized by the periodically spaced potential field. The total electron energy equals the sum of the transverse energy and

†Corresponding author. E-mail: chenjunfeng.cjf@gmail.com

the vertical energy which is calculated by the tight binding (TB) method, considering the coupling of the wave function between the nearest wells[13]

$$\varepsilon(k) = \varepsilon_{k\parallel} + \varepsilon_{kz} \tag{1}$$

with

$$\varepsilon_{kz} = \frac{1}{2}\Delta(1 - \cos(k_z \cdot d)), \tag{2a}$$

where Δ is the width of the lowest miniband, d is the superlattice period (well add barrier). k_z is the wave vector in the z direction. GaN based material has a strong polarization effect. For a short period AlGaN/GaN superlattice, its saw shape band edge oscillation (shown in Fig.1) differs from the rectangular shape band edge oscillation of an AlGaAs/GaAs superlattice. The saw shape band edge oscillation is caused by piezoelectric polarization induced by the interface misfit between the AlGaN and GaN layers. The penetration coefficient of the wave function in the short triangular well is greater than that in the rectangular well, thus it is not precise enough to calculate the energy dispersion relation just using the nearest wells in TB method. More wells must be accounted for in this situation. We use parameter γ to describe the coupling coefficient of the next nearest wells. The magnitude of the coefficient γ depends on the extent of wave fuction overlap and does not exceed 0.2 even for a superlattice as short as $d = 2.2$ nm. Then the vertical energy dispersion relation can be rewritten as in Eq.(2b).[14] In comparison with Eq.(2a), the new relation includes the effect of the $2kz$ term

$$\varepsilon_{kz} = \frac{1}{2}\Delta[1 - \gamma - (\cos(k_z \cdot d) - \gamma\cos(2k_z \cdot d))]. \tag{2b}$$

The calculated result of the energy dispersion relation is shown in Fig.2, with period $d = 2.4$ nm and $\Delta = 140$ meV. From Fig.2 we can see that with the increase of the coupling coefficient γ, the energy dispersion relation departs gradually from the simple cosine relation. The curvature at the centre of the Brillouin zone is smaller than that of the simple cosine relation. Therefore, the conduction electron effective mass is bigger than that of a traditional result. The following calculations and discussions are all based on this improved energy dispersion relation.

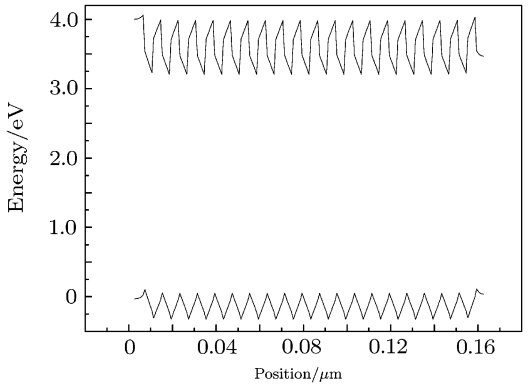


Fig.1. Band edge oscillation of AlGaN/GaN SLs.

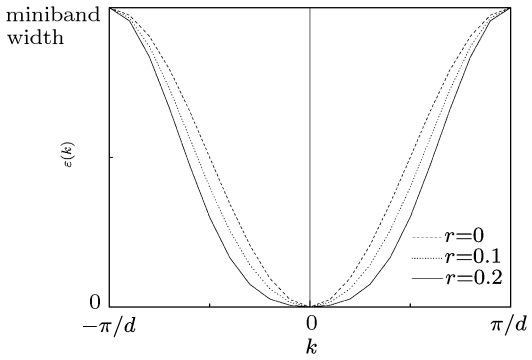


Fig.2. Energy dispersion relation of a miniband electron in AlGaN/GaN SLs.

2.2. Electron group velocity under a static electric field

Treating the electron as a wave packet with the centre wave vector k, the group velocity of the wave packet can be described as

$$v_{\mathrm{g}} = \frac{1}{\hbar}\frac{\partial\varepsilon}{\partial k}. \tag{3}$$

The phase of the wave packet is

$$\varphi = kd. \tag{4}$$

Under an electric field along the superlattice growth direction, electrons are accelerated by this field. The force of an electron taken is

$$\hbar\dot{k} = eE(t). \tag{5}$$

By integrating Eq.(5) and substituting it into Eq.(4), the phase can be rewritten as

$$\varphi = kd = \int_{t0}^{t}\frac{ed}{\hbar}E(t')\mathrm{d}t'. \tag{6}$$

Substituting Eq.(6) into Eq.(3) and using the energy dispersion relation Eq.(2b), the group velocity is given by

$$v_{\mathrm{g}} = \frac{\Delta d}{2\hbar}\sin\int_{t0}^{t}\frac{ed}{\hbar}E(t')\mathrm{d}t' \times\left(1 - 4\gamma\cos\int_{t0}^{t}\frac{ed}{\hbar}E(t')\mathrm{d}t'\right). \tag{7}$$

When the electric field is a static field $E(t) = E_s$, equation (7) can be simplified as

$$v_g = \frac{\Delta d}{2\hbar} \sin\omega_b(t-t_0)(1-4\gamma\cos\omega_b(t-t_0)), \quad (8)$$

where $\omega_b = edE_s/\hbar$ is the Bloch angular frequency. In one period an electron is accelerated by the static electric field until it reaches the upper band edge, then it undergoes Bragg reflection and decelerates to the initial energy. Suppose that P is the collision probability that an electron does not undergo collision from time t_0 to t; then P can be written as

$$P = \frac{1}{\tau}\exp\left(-\frac{t-t_0}{\tau}\right), \quad (9)$$

where τ is the electron overall relaxation time. At room temperature, the dominant relaxation process in bulk GaN is associated with polar optical phonons.[15,16] The relaxation time in this paper is based on the intersubband scattering time estimated for AlGaN/GaN quantum wells.[17,18] The relaxation time 0.25 ps is taken in our calculation.

From Eqs.(9) and (7) the electron drift velocity is obtained:

$$v(t) = \int_{-\infty}^{t} \frac{1}{\tau}\exp\left(-\frac{t-t_0}{\tau}\right) v_g \mathrm{d}t_0. \quad (10)$$

In a static electric field, using Eq.(8), equation (10) can be rewritten as

$$v_s = \frac{1}{\tau}\frac{\Delta d}{2\hbar}\left(\frac{\tau^2\omega_b}{1+\tau^2\omega_b^2} - 2\gamma\frac{2\tau^2\omega_b}{1+4\tau^2\omega_b^2}\right), \quad (11)$$

making $E_c = \hbar/ed\tau$ and $v_p = \Delta d/4\hbar$, equation (11) can be simplified as

$$v_s = 2v_p\left(\frac{E_s/E_c}{1+(E_s/E_c)^2} - 4\gamma\frac{E_s/E_c}{1+4(E_s/E_c)^2}\right). \quad (12)$$

By comparing this result with that from the traditional simple cosine relation,[19] the second term is a new additional term causing anharmonic electron oscillations at the multiples of the fundamental Bloch frequency. Figure 3 shows the relations of the electron drift velocity under a static electric field E_s with various coupling coefficients γ. When $\gamma = 0$, at the region from $-E_c$ to E_c, the drift velocity increases quasi-linearly as $v_d \approx u \cdot E_s$, this is the Ohmic resistance region. In the region of $E_s > E_c$ and $E_s < -E_c$, the drift velocity decreases, which is the negative resistance region. When γ increases, the peak drift velocity becomes smaller, and the electric field E_s is larger at the peak velocity. When $\gamma = 0.1$ and 0.2, the peak velocity is 84% and 70% of the value at $\gamma = 0$. Furthermore, when $\gamma = 0.2$ the linear Ohmic region $-E_c < E_s < E_c$ can be divided into two linear regions $E_s < |0.3E_c|$ and $|0.3E_c| < E_s < |E_c|$. The velocity slope in the first region is smaller than that in the second region, which means that the Ohmic resistance is smaller at $E_s < |0.3E_c|$ than at $|0.3E_c| < E_s < |E_c|$. This phenomenon is caused by the anharmonic term in the energy dispersion relation. This semiclassical theory is concise and acceptable for depicting the effects of the overall relaxation time on the nonlinear transport characteristic, but it cannot be used to investigate the specific transport mechanism in detail. When $\gamma = 0$ the drift velocity agrees with the result derived from one-dimensional Boltzmann theory in the relaxation time approximation.[20]

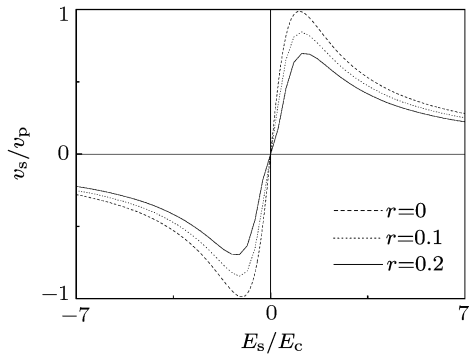


Fig.3. Drift velocity under a static field.

2.3. Drift velocity of a miniband electron under an ac electric field

Consider a dc electric field E_0 and a cosine ac field of frequency ω and amplitude $E\omega$ as:

$$E(t) = E_0 + E\omega\cos(\omega t). \quad (13)$$

Substituting Eq.(13) into Eq.(7), the drift velocity of the steady state under $E(t)$ is obtained:

$$v(t) = \int_{-\infty}^{t} \frac{1}{\tau}\frac{\Delta d}{2\hbar}\exp\left(-\frac{t-t_0}{\tau}\right) \times\left[\sin\int_{t_0}^{t}\frac{ed}{\hbar}E(t')\mathrm{d}t' \times\left(1-4\gamma\cos\int_{t_0}^{t}\frac{ed}{\hbar}E(t')\mathrm{d}t'\right)\right]\mathrm{d}t_0. \quad (14)$$

An AlGaN/GaN superlattice structure with period $d = 2.4$ nm and $\Delta = 140$ meV to an applied field of frequency $f = 1$ THz, $E_0 = 3E_c$ and $E\omega = 3E_c$ is considered. The calculated steady time-dependent

response in one period of the transient drift velocity after eliminating a time delay of a few picoseconds from turning on the applied THz field $E(t)$ is shown in Fig.4. Compared with the drift velocity at $\gamma = 0$, the peak drift velocity at $\gamma = 0.2$ is 10% larger and the peak velocity reaches 0.03 picoseconds earlier, which almost equals $\pi/16$ earlier in the phase. Figures 3 and 4 show clearly that the coupling effect in the short period AlGaN/GaN superlattice plays an important role in the electron transport characteristics.

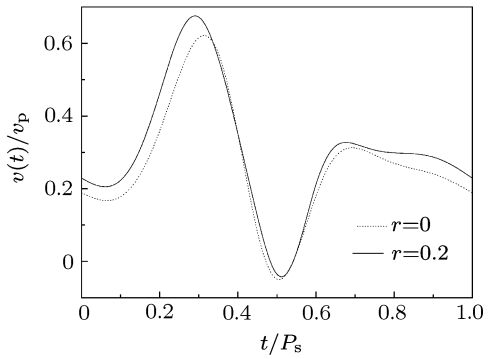


Fig.4. Steady time-dependent response of the drift velocity under $E(t) = 3E_c + 3E_c\cos(\omega t)$ at $f = 1$ THz.

3. Harmonic analysis and discussion

A superlattice is a nonlinear element that responds to an ac electric field not only at the principal frequency but also at higher harmonics. From Eq.(14), it can be seen that the drift velocity is a periodic time function with period $T\omega = 1/f$, thus the drift velocity of the steady state can be expanded in the form of a Fourier series consisting of dc and different harmonic components:

$$v_d(t) = v_{d0} + \sum_{n=1}^{\infty} [v_{dn1}\cos(n\omega t) + v_{dn2}\sin(n\omega t)], \tag{15}$$

where the dc component and the harmonic components are given by

$$v_{d0} = \frac{1}{T}\int_0^T v_d(t)\mathrm{d}t, \tag{16a}$$

$$v_{dn1} = \frac{2}{T}\int_0^T v_d(t)\cos(n\omega t)\mathrm{d}t, \tag{16b}$$

$$v_{dn2} = \frac{2}{T}\int_0^T v_d(t)\sin(n\omega t)\mathrm{d}t. \tag{16c}$$

An $Al_{0.4}Ga_{0.6}N/GaN$ superlattice with period $d = 2.4$ nm, miniband width $\Delta = 140$ meV and coupling coefficient $\gamma = 0.15$ is used in the following calculation. In this structure, the peak drift velocity $\nu_p = 1.1\times10^7$ cm/s, $E_c = 13.2$ kV/cm. Figure 5 shows the calculated real part amplitude of the steady drift velocity of the first 10 odd order harmonic components at $f = 1$ THz, $E_0 = 0$ and $E\omega = 5E_c$. In this zero biased case, the dc component and all the even order harmonic amplitudes of the steady drift velocity are zero. The amplitude of the odd order harmonic components decreases rapidly with increasing harmonic order. The first and the second harmonic components are positive, while the other harmonic components are negative or almost zero. Figure 6 shows the relation between the real part amplitude of the first, third, fifth, seventh order harmonic components and the ac electric field strength at $f = 1$ THz and $E_0 = 0$. The first harmonic component reaches its peak value at about $3.4E_c$ then decreases rapidly, the amplitudes of the third, fifth, seventh order harmonic components oscillate and increase gradually with the increase of ac field strength $E\omega$.

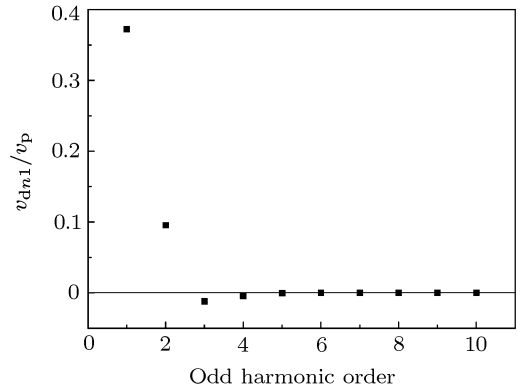


Fig.5. Calculated real parts of the first 10 odd order harmonics.

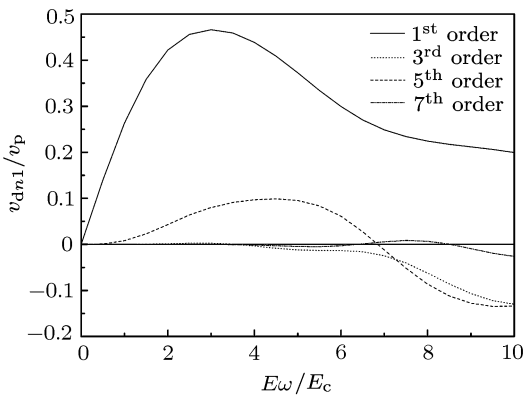


Fig.6. Real parts of the first, third, fifth and seventh order harmonic components.

Figure 7 shows the relation of the real part amplitude of the third harmonic component with the electric field strength E_0 and $E\omega$, at $f = 1$ THz. When the ac field is low the dc field can suppress the third harmonic amplitude. The peak amplitude is reached at $E_0 = 1$ and $E\omega = 5E_c$. With increasing E_0, the peak amplitude decreases and shifts to the high side of the $E\omega$ axis. The threshold $E\omega$ for the nonzero amplitude increases as well. As a complement, the role of the ac field frequency to the third harmonic amplitude accompanied by the ac field strength $E\omega$ is calculated and shown in Fig.8. With increasing ac field strength, the third amplitude varies from positive to negative. At the low side of the frequency $f = 100$ GHz, the amplitude decreases to a valley at first and then increases as follows. At the high side, the amplitude will increase to a peak value at first and then the amplitude decreases rapidly to the valley point. In comparison with the low frequency side, the valley shifts to the high side of the $E\omega$ axis.

The dependence of the phase shift of the third harmonic component on the ac field frequency f and the ac field strength $E\omega$ at $E_0 = 0$ is calculated and plotted in Fig.9. It can be seen that there exists a critical ac field strength and frequency. When ac field strength and frequency exceed the critical value, the third harmonic phase will increase to about π at first and then drop dramatically to about $-\pi$. At last the phase will tend to $-\pi/2$ at the high side of the ac field. As a promising THz source the power efficiency is an important parameter, the relative power efficiency of the third harmonic as a function of the dc and ac field strength is calculated and illustrated in Fig.10. The power of the third harmonic is proportional to $(v_{d32}^2 + v_{d31}^2)$ and the input power of ac field is proportional to $E\omega^2$, thus the relative power efficiency can then be described by $(v_{d32}^2 + v_{d31}^2)/E\omega^2$. As shown in Fig.10 the maximum relative power efficiency is obtained at $E_0 = 3E_c$ and $E\omega = 4E_c$, the second peak is at about $E_0 = 0$ and $E\omega = 7E_c$. At other points which deviate from the peak the relative power efficiency drops to almost zero. Thus the $E_0 = 3E_c$ and $E\omega = 4E_c$ configuration seems more efficient to use as a frequency multiplicator of 3ω.

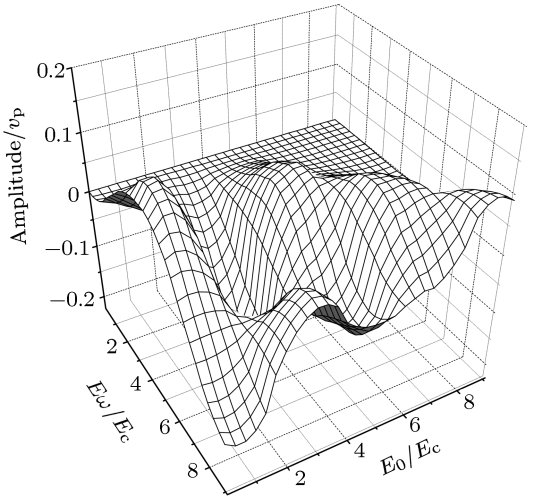


Fig.7. Relation of the third harmonic amplitude with ac and dc field strengths.

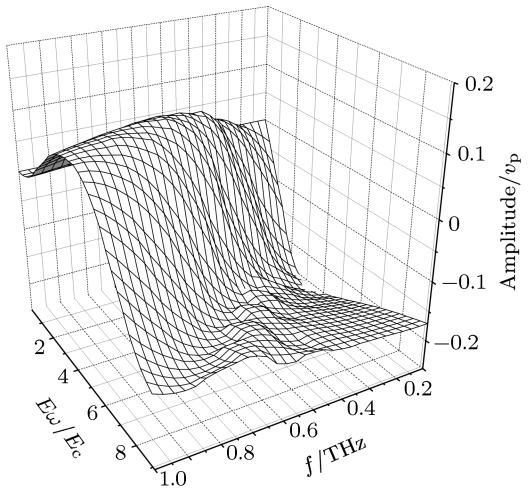


Fig.8. Relation of the third harmonic amplitude with ac field strength and frequency.

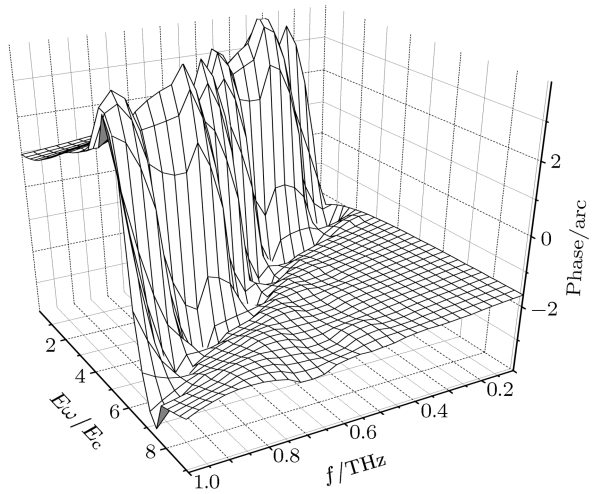


Fig.9. Relation of the third harmonic phase shift with ac strength and frequency.

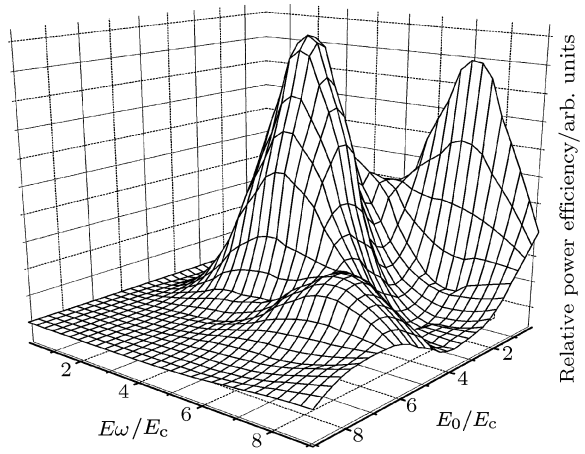


Fig.10. Relation of the third harmonic relative power efficiency with ac and dc strengths.

4. Conclusion

Benefiting from the high critical field and the thermal conductivity, THz devices fabricated by GaN material can supply a higher output power density and suffer from higher operation temperature. In this paper, based on the improved energy dispersion relation the harmonic components of short period AlGaN/GaN superlattice miniband electron drift velocity under a THz electric field is investigated. To a short period AlGaN/GaN superlattice, the coupling effects on the energy dispersion cannot be negligible. The calculated drift velocity is 30% smaller under a dc field and 10% larger under an ac field than the results taking no account of the coupling effects. Both the field strength and the field frequency play important roles in the harmonic amplitude, phase and relative power efficiency. The maximum relative power efficiency is obtained at about $E_0 = 3E_c$ and $E\omega = 4E_c$. These results show that the AlGaN/GaN superlattice is a promising candidate to convert radiation of frequency ω to radiation of frequency 3ω or even higher.

References

[1] Kawase K, Ogawa Y and Watanabe Y 2003 *Opt. Express* **11** 2549
[2] Yen T J, Padilla W J and Fang N 2004 *Science* **303** 1494
[3] Wang S H, Ferguson B, Zhang C L and Zhang X C 2003 *Acta Phys. Sin.* **52** 120 (in Chinese)
[4] Liu H, Xue D G and Yao J Q 2009 *Chin. Phys.* B **18** 1077
[5] Trew R J 2005 *IEEE Trans. Electron Devices* **52** 638
[6] Foutz B E, Eastman L F and Bhapkar U V 1997 *Appl. Phys. Lett.* **70** 2849
[7] Kolnik J, Oguzman I, Brennan K F, Wang R P, Ruden P P and Wang Y 1995 *J. Appl. Phys.* **78** 1033
[8] Krishnamurthy S, Schilfgaarde M V and Scher A 1997 *Appl. Phys. Lett.* **71** 1999
[9] Kohler R, Tredicucci A, Beltram F, Beere H E, Linfield E H, Davies A G, Ritchie D A, Iotti R C and Rossi F 2002 *Nature* **417** 156
[10] Williams B S, Kumar S, Hu Q and Reno J L 2006 *Electron. Lett.* **42** 89
[11] Kumar S, Williams B S, Hu Q and Reno J L 2006 *Appl. Phys. Lett.* **88** 121123
[12] Williams B S, Kumar S, Hu Q and Reno J L 2005 *Opt. Express* **13** 331
[13] Esaki L and Tsu R 1970 *IBM J. Res. Develop.* **14** 61
[14] Litvinov V I, Manasson A and Pavlidis D 2004 *Appl. Phys. Lett.* **85** 600
[15] Shur M, Gelmont B and Asif Khan M 1996 *J. Electron. Mater.* **25** 777
[16] Zanato D, Gokden S, Balkan N, Ridley B K and Schaff W J 2003 *Superlatt. Microst.* **34** 77
[17] Ng H M, Gmachl C, Frolov S V, Chu S N G and Cho A Y 2001 *IEEE Proc. Optoelectron.* **145** 215
[18] Heber J D, Gmachl C, Ng H M and Cho A Y 2002 *Appl. Phys. Lett.* **81** 1237
[19] Renk K F, Rogl A and Stahl B I 2007 *J. Luminescence* **125** 252
[20] Ignatov A A, Schomburg E, Grenzer J, Renk K F and Dodin E P 1995 *Z. Phys.* B **98** 187